Multi-Planar Plenoptic Displays

Nicola Ranieri
ETH Zürich

Simon Heinzle
Disney Research Zurich

Peter Barnum
Disney Research Zurich

Wojciech Matusik
CSAIL, MIT

Markus Gross
Disney Research
ETH Zürich

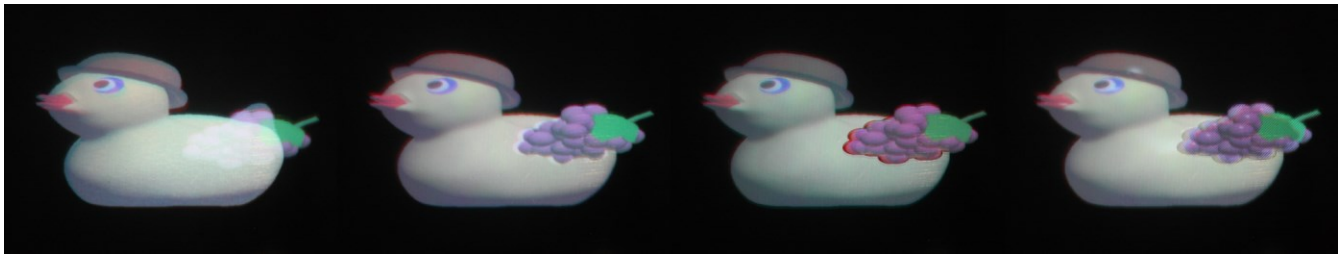

Figure 1: Illustration of the steps of our light field decomposition. (1) volumetric rendering, (2) view-independent and (3) view-dependent occlusion culling, (4) view-dependent rendering on parallax type layer. Photographs are taken from our multi-layered display prototype.

Abstract

Multi-planar plenoptic displays consist of multiple spatially-varying light emitting and light modulating planes. In this work, we introduce a framework to display light field data on this new type of display device. First, we present a mathematical notation that describes each of the layers in terms of the corresponding light transport operators. Next, we explain an algorithm that renders a light field with depth into a given multi-planar plenoptic display and analyze the approximation error. We show two different physical prototypes that we have designed and built: The first design uses a dynamic parallax barrier and a number of bi-state (translucent/opaque) screens. The second design uses a beam-splitter to co-locate two pairs of parallax barriers and static image projection screens. We evaluate both designs on a number of different 3D scenes. Finally, we present simulated and real results for different display configurations.

Author Keywords

3D display; light field decomposition; multi-planar; plenoptic function; display primitives; light transport.

1. Introduction

Glasses-free 3D displays have experienced a major renaissance in the past few years. In general, these displays can be divided into two main categories: parallax-based displays and volumetric displays. Parallax-based approaches such as integral imaging [11] and parallax barriers [8] redirect spatially varying pixels onto different viewing directions. These approaches trade off spatial resolution in favor of angular resolution, which directly relates to the depth range that can be displayed without aliasing [4]. Though being capable of view dependent effects and proper occlusions, these devices often exhibit low spatial or angular resolution and lack correct accommodation cues. Volumetric displays [[5],[9],[13]], on the other hand, physically deploy light-emitting voxels in 3D space and provide a direct and natural approximation of the input scene. They provide correct accommodation cues but are, with few exceptions, not capable of providing proper occlusions or view dependent effects. A comprehensive overview of volumetric displays is given in [7].

As alternative, multi-planar displays [[1],[2],[12],[14],[15]] have been suggested to provide natural ways to show 3D scenes at nearly correct accommodation cues with increased display bandwidth and hence higher angular and spatial resolution. In essence, these displays combine parallax and volumetric displays and draw benefits from both. In our work, we generalize these concepts to multi-planar plenoptic displays by defining basic display layer primitives, consisting of emissive and modulating layers. We provide a mathematical framework to describe light transport through any combination of such layers. Based on this framework, we then provide a method to distribute an input light field according to a given display configuration. Furthermore, a quantitative error analysis for different layer configurations is provided. Finally, we present two physical prototypes, capable of rendering volumetric content with view dependent effects, proper occlusions and better accommodation cues and we show results for both of them.

2. Mathematical Framework

Our model assumes co-planar display layers which are aligned with the *xy* plane. Each of the layers can either be emitting or modulating, performing a certain operation on the overall light transport which will be described in the following.

Our model is using a similar notation and concepts as presented by Durand et al.[6]. In general, the light field ℓ describes the radiance of light rays passing through points (x,y) and (u,v) at distance z from the xy plane, and is denoted as $\ell(x,y,z,u,v)$. For simplicity, we will only consider light rays traveling along the positive z direction, as our displays will only be viewed from the front.

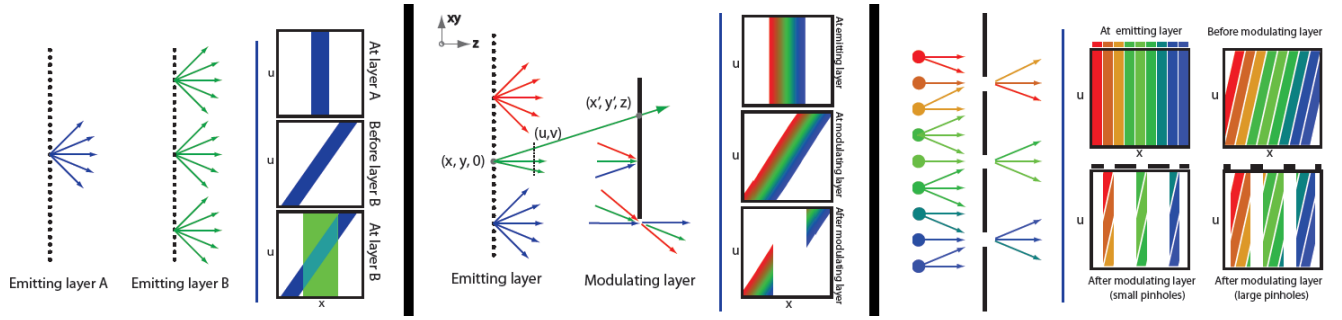

Figure 2: The three basic display layer primitives. Overlay of two emissive layers is shown on the left, impact of a modulating layer in the middle and the principle of a parallax barrier layer on the right.

Light Transport in Free Space: The basic light transport is illustrated in Figure 2 (middle). A ray starting at position *(x,y,z)* passing through *(u,v)* traverses in free space to

$$x' = x + \Delta z \cdot u,\ y' = y + \Delta z \cdot y$$

As the ray moves in depth, its position will change to $(x',y',z+\Delta z)$ while keeping its original traveling direction *(u,v)*.

Display Layer Primitives: Many of the display layer types deployed in modern systems can be generalized to two categories. We describe both categories as basic display primitive and provide a mathematical notation for the light transport operator. Together with the notation of light transport in free space, more complex systems made of any combination of such display primitive layers can be described.

Emissive Layer: An emissive layer E acts like an array of point light sources, emitting constant spherical light. We use the notation $Ez(x,y)$ as the light portion at x and y on the plane at depth z, radiating into all directions *(u,v)*. The emissive layer adds light to an input light field ℓi, and yields the output light field ℓo, as illustrated in Figure 2 on the left:

$$\ell o(x,y,z,u,v) = \ell i(x,y,z,u,v) + Ez(x, y)$$

Opaque emissive layers can be found in any 2D display consisting of e.g. a backlight with a modulating color LCD. However, to optically overlay them with other display layer primitives, transparent emitters are preferred. This can be implemented using the upcoming transparent OLED technology, by transparent back-projection foils or, as in our prototype, polymer dispersed liquid crystal (PDLC) layers in combination with a projector.

Modulating Layer: A spatial modulating plane M will gradually attenuate all rays *(u,v)* passing through a certain pixel *(x,y)*. The modulating layer $Mz(x,y)$ is therefore represented as scalar between zero and one, and the output light field can be described as:

$$\ell o(x,y,z,u,v) = \ell i(x,y,z,u,v) \cdot Mz(x,y)$$

The operation is shown in Figure 2 in the middle. Modulating layers can be implemented by (grayscale) liquid crystal displays, as the polarization rotation capability of twisted nematic liquid crystals can be used to block light when combined with two polarizers.

Parallax Barrier Layer: Parallax barrier displays are basically a combination of an emissive layer and a modulating layer with a special modulating pattern and small spacing Δz between the two layers. Therefore, the same light transport operators as for above layers are used. Since this pairing is fundamental, we define it as third basic primitive shown in Figure 2 on the right. The modulating layer is used to achieve ray separation by displaying a vertical slit, diagonal slit or pinhole pattern, while the emissive layer displays the different rays that pass through the slits/pinholes. As a consequence, an observer will see different rays from different directions. N pixels on the emitter plane can be partitioned into any number of spatial and angular samples *(x,y,u,v)*, such that $N > x \cdot y \cdot u \cdot v$. In practice, such displays trade a substantial reduction of spatial resolution for a relatively small amount of rays and apparent depth. The work of Levin et al. [10] provides a good background on this subject.

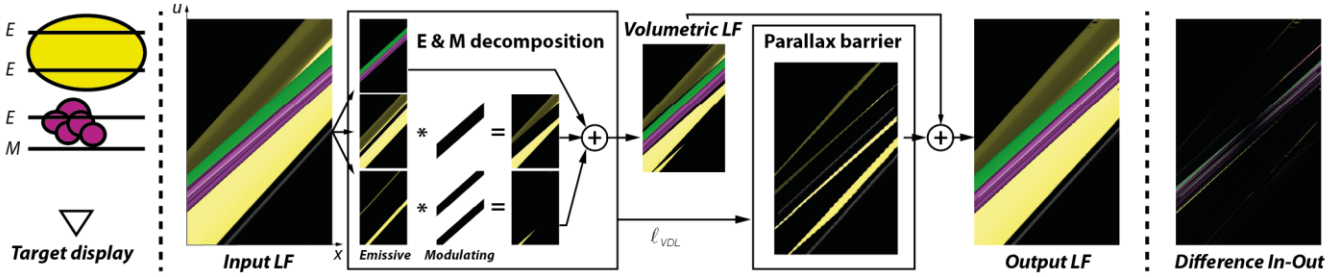

Figure 3: Illustration of the decomposition algorithm for a display layer configuration of one front-most modulating layer followed by three emissive layers. View independent emissive elements are assigned, occlusions computed and the residue added using parallax barrier rendering.

3. Light Field Decomposition

Based on the analysis in the previous section, we will describe an algorithm that approximates an input light field $\ell i(x,y,z,u,v)$ as an output light field $\ell o(x,y,z,u,v)$ targeted for a given multilayer plenoptic display D_i. Our algorithm decomposes the input light field into a number of components. Each component is then displayed on one or multiple display primitives. In order to aid the decomposition process, we assume that for all rays (x,y,z,u,v) of the input light field we know the depth z of the closest object, the diffuse component R_D, and the specular/glossy component R_S.

More specifically, the algorithm separates the light field data into planar components. First, the view-independent volumetric components ℓ_{VIV} are extracted from the light field, i.e. ℓ_{VIV} will contain the rays that are not occluded at any angle. Next, a view-dependent partially occluded volumetric part ℓ_{VDV} is extracted. Finally, the remaining light field ℓ_{VDL} is extracted for rendering with parallax barrier layers. Algorithm 1 gives a high level overview of how to generate $\ell o(x,y,z,u,v)$ from an input light field $\ell i(x,y,z,u,v)$ for a given display setup D_i. Example decomposition is given in Figure 3.

Algorithm 1: High level overview of the rendering algorithm

$\ell_{VIV} \leftarrow assignViewIndependentVolumetric(\ell i, D_i)$

$\ell_{residue} \leftarrow \ell i - \ell_{VIV}$

$\ell_{VDV} \leftarrow assignViewDependentVolumetric(\ell i, \ell_{residue}, D_i)$

$\ell_{residue} \leftarrow \ell_{residue} - \ell_{VDV}$

$\ell_{VDL} \leftarrow assignViewDependentLightField(\ell_{residue}, D_i)$

$\ell_{residue} \leftarrow \ell_{residue} - \ell_{VDL}$

In a first step all diffuse components not occluded from any viewing angle are extracted from the light field. The extracted components are then distributed onto the available emitting layers. Only components that are spatially close enough to the emitting layers are considered for display, to minimize the re-projection error. More specifically, each part of R_D that is within a distance z_{thresh} from any layer is assigned to the nearest layer in the display setup D_i. Assignment is performed by parallel projection. The parts of R_D that are further than z_{thresh} from all layers are not processed and left as residue for the automultiscopic display layers. Algorithm 2 summarizes this procedure.

Algorithm 2: $\ell_{VIV} \leftarrow assignViewIndependentVolumetric(\ell i, D_i)$

```
for emissiveLayer ϵ Di
    for x, y, z, RD ϵ ℓi
        dz ← distance([x, y, z], emissiveLayer)
        if RD ≠ 0 and dz < zthresh and notOccluded(x, y, z)
            emissiveLayer[x, y] ← RD
            ℓVIV.add([x, y, z, RD])
```

In a second step shown in Algorithm 3, diffuse components which are partially occluded are assigned to emissive layers and properly occluded by a modulating layer. Optimally, each emissive layer is preceded by a modulating layer to provide correct occlusions. However, as in practice modulating layers often absorb much light also in their transparent state, a fewer number of modulating layers is desired. For each emissive pixel, occlusions for all emissive layers in front are detected, and the modulating layer closest to but behind the occluding layer is used for masking. The occlusion mask is retrieved by intersecting the ray from the emissive pixel to its occluding pixel with the chosen modulating layer. This step creates black borders (illustrated in the third image in Figure 1 or the bottom of Figure 5) since occlusions are detected conservatively over the whole viewing angle. Therefore, such over-occlusions have to be added back to the residue, as they have to be rendered as view dependent light field.

Algorithm 3: $\ell_{VDV} \leftarrow assignViewDependentVolumetric(\ell i, \ \ell_{residue}, D_i)$

```
for emissiveLayer ϵ Di
    for x, y, z, RD ϵ ℓresidue
        dz ← distance([x, y, z], emissiveLayer)
        if RD ≠ 0 and dz < zthresh
            emissiveLayer[x, y] ← RD
            ℓVDV.add([x, y, z, RD])
            for x', y', z' ϵ ℓi
                if occludes([x, y, z], [x', y', z'])
                    modulator ← getClosestModulator([x', y', z'])
                    modulator.occlude([x, y, z], [x', y', z'])
for modulator ϵ Modulators
    for u, v ϵ modulator:OccludedPixels()
        ℓVDV.removePartsOccludedBy(modulator[u; v], ℓi)
```

In a last step, the residue has to be rendered, filling the black borders and adding other view-dependent light field portions. Due to the planar mapping to the emissive layers, the holes cannot be filled naively. Our solution stretches the occluded residual to match the gap borders as illustrated on the left hand side of Figure 4, which corresponds to a scale in depth as shown on the right hand side. The same has to be considered for the glossy parts: They are mapped to the same plane as the view independent/diffuse part before being rendered. All components of this third step shown in Algorithm 4 are rendered using the closest parallax barrier layer and have to be filtered accordingly using existing approaches [16]. A result of the complete algorithm is shown on the right of Figure 1.

Algorithm 4: $\ell_{VDL} \leftarrow assignViewDependentLightField(\ell_{residue}, D_i)$

```
for x, y, z, RD, RS ϵ ℓresidue
    if RD(x, y, z) on emissiveLayer ϵ Di
        project RS(x, y, z, u, v) onto RS(x, y, emissiveLayer.z, u, v)
Perform hole filling for continous surfaces: WarpResidue( ℓresidue )
for x, y, z, RD, RS ϵ ℓresidue
    lightfieldLayer ←getClosestLightFieldLayer(x, y, z)
    lightfieldLayer[x, y, u, v] ← RD + RS
    ℓVDL.add([x, y, z, u, v, RD , RS ])
```

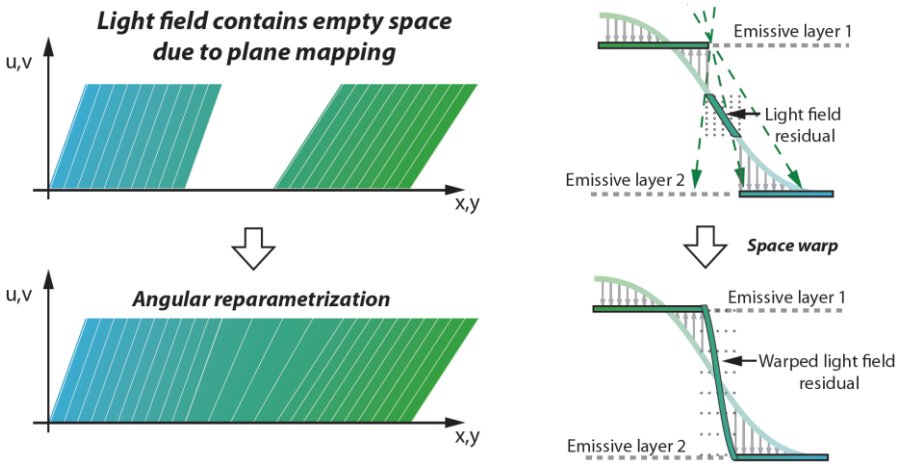

Figure 4: Adaptive hole filling between emissive layers.

4. Decomposition Analysis

We analyze our system with respect to the projective error, the error introduced by the sampling in the light field layer and a quantitative error measurement.

Projective Error: The projection onto the planar emitters inherently produces an approximation of the motion parallax. The motion parallax produced by an object at distance z to a viewer with focal length f that moves along a baseline at a distance b can be expressed as

$$d = -f \cdot b / z$$

We express the relative projective approximation error of an object at distance z projected on a plane at distance z_0 by

$$e(z, z_0) = |1/z_0 - 1/z|$$

The emissive layers should therefore ideally be placed near dense occurrences of objects in depth, and the occluding layers should be placed as near as possible to the respective layers that need occlusion. Furthermore, fewer display elements are needed the farther the scene is with respect to the viewer's position. This error can be used to determine the optimal display configuration using a suited optimization method, in cases where a display configuration is optimized for a given scene.

Light Field Sampling Error: Light field layers usually trade off spatial against angular resolution, and the approximation error is directly proportional to the loss in spatial resolution. However, additional errors are introduced if aliasing occurs when the angular frequencies are too high. These problems can be overcome by either using time-multiplexing for the parallax barrier display, or by combining multiple parallax barrier displays superimposed onto the same optical path. Latter approach has further the advantage, that the required bandwidth for each light field layer is decreased by $1/n^2$, with n the number of layers, resulting in a total required bandwidth of $1/n$, as described in [12].

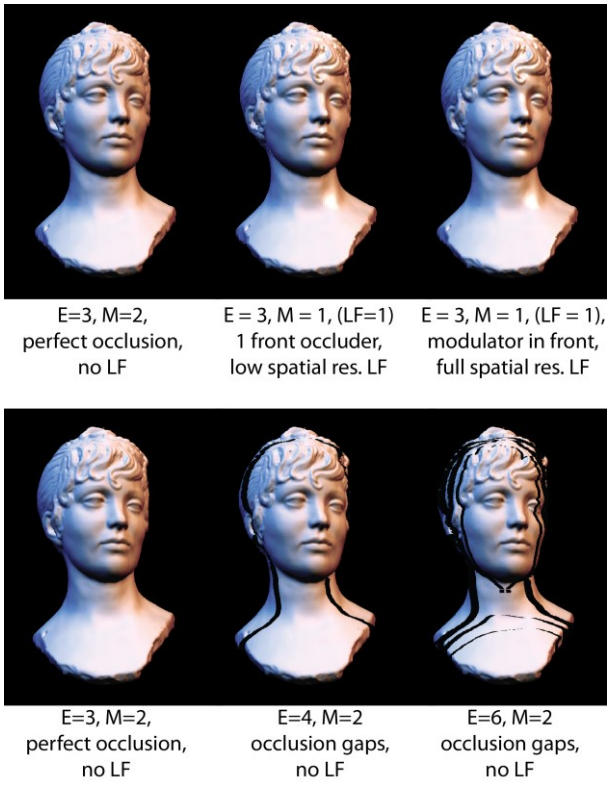

Figure 5: Simulated results used for the quantitative error analysis.

Quantitative Error: To analyze the impact of number of layer primitives, we compare the resulting reprojection errors using our software simulation. We simulated two different scenes: a duck scene containing two objects at different depths with occlusion, and a bust scene depicting a continuous surface. Both scenes contain a small amount of specular highlights. The simulated results are compared to a perfect rendering, and the MSE between the simulated and perfect images are computed for a number of views in a field of view of 15°. The resulting error plots are shown in Figure 6.

In the left plot, the impact of an increasing number of emissive layers is depicted for three cases: In a first case, each emissive layer is preceded by a modulating layer, providing perfect occlusions for scene content in the back (red plots). In a second and third case, only one modulating layer is deployed front most and view dependent content is added by low resolution (green plots) or full resolution (blue plots) light field rendering. The error decreases fast when adding the first few layers, however, adding more than 4 layers does not reduce the error as drastically anymore.

In the right plot, the impact of an increasing number of modulating layers is assessed for a fix number of six (red plots), four (green plots) and three (blue plots) emissive layers. For this analysis, the modulating layers are placed after each emissive layer, starting from the front-most layer. An increasing number of modulating layers helps to reduce the error significantly. The plots furthermore show that increasing the number of emissive layers without increasing the number of modulating layers leads to significant high errors due to incorrect occlusions, perceived as black gaps as shown in Figure 5 on the bottom.

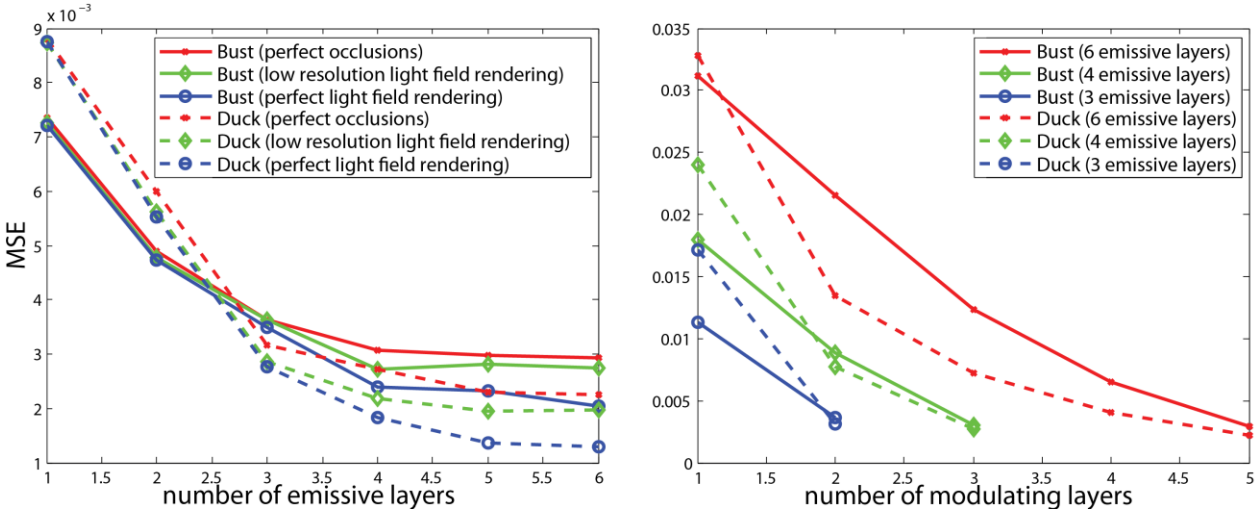

Figure 6: Quantitative error analysis using simulated results. Impact of an increasing number of emissive (left) as well as modulating layers (right) is evaluated.

5. Implementation

Based on the analysis presented in the previous section, we implemented two types of multi-layer plenoptic displays. Our two setups are shown in Figure 8 and Figure 9. The first prototype uses temporal multiplexing to superimpose the different layers, while the second uses spatial multiplexing. Temporal multiplexing is performed by combining a projector with multiple bi-state scattering planes. Spatial multiplexing is performed by combining two automultiscopic displays using a beam splitter.

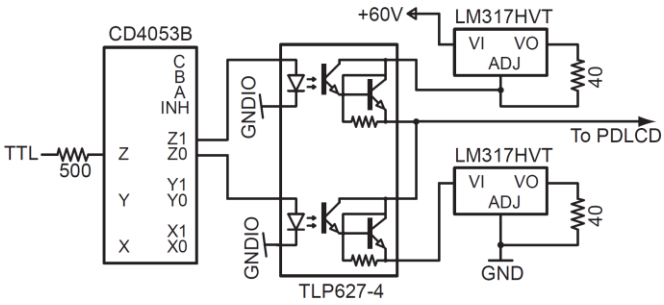

Figure 7: Circuitry used to create an alternating square wave function to drive the PDLC layers.

Display Prototype using temporal multiplexing: We provide an example configuration in a first, temporally multiplexed prototype. It deploys three PDLC layers in combination with a projector to approximate the emissive layer primitive, and a LCD in the front as modulating layer. In each frame, one of the PDLC layers is opaque and diffuses incoming light while the others are transparent. This allows showing different images on different layers in time-multiplexed manner, similar to [13]. The PDLC layers are driven by the circuitry shown in Figure 7 which creates an alternating square wave function, preserving damages to the liquid crystal structures. The circuitry is synchronized with the v-sync signal of the projector such that the opaque layer is switched with each newly projected frame. As modulating layer, we employ an LCD with non-diffusing polarizing films. This layer is front most and used both to provide approximated occlusion as well as to render the light field portion of our decomposition algorithm.

The PDLC layers are spaced at 4mm, 10mm and 16mm from the front LCD. The projector has XGA resolution and a refresh rate of 60Hz, matching the refresh rate of the used PDLC layers. The front LCD renders 12 views in a 10° field of view when used as parallax barrier layer. The effective refresh rate of the display is 15Hz, since the front most emissive layer is used both for volumetric rendering as well as for parallax barrier rendering. The complete setup is shown in Figure 8.

Multi-planar plenoptic displays with homogeneous and well-aligned optical elements do not require calibration, since pixels are stacked directly behind each other in a one-to-one correspondence. However, in our setup we combine heterogeneous elements such as the projector and the LCD, which makes software calibration necessary. We propose a variant of the calibration scheme proposed in [1], and perform homography estimation based on photographs of projected checkerboard patterns.

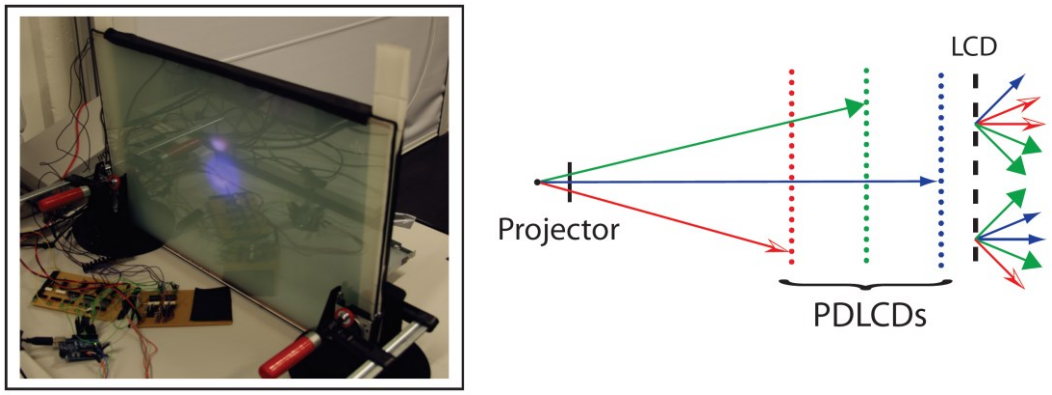

Figure 8: Our temporally multiplexed prototype consists of three emissive layers and a front most modulating layer.

Display Prototype using spatial multiplexing: Our second prototype combines two automultiscopic parallax barrier displays using spatial multiplexing. The parallax barriers are only used for 3D light-fields, i.e. the barriers only provide distinct rays aligned with the horizontal plane. Both displays are combined onto the same optical path using a beam-splitter mirror. Each of the displays is placed at a different distance from the beam splitter and is then used to display different parts of the light field to achieve increased depth range. Each parallax barrier display is composed of a 120 Hz projector paired with a diffuse back-projection layer for the emissive primitive and a TN-LCD displaying a parallax barrier pattern as modulating primitive. Parallax barrier displays usually require big spacing between the barrier stripes to achieve an acceptable angular resolution. They therefore result in spatially under-sampled images that additionally lack a considerable amount of brightness due to the pin-hole nature of the barrier. We therefore employ temporal multiplexing for each barrier display: multiple spatially offset barrier patterns are projected in short sequence, with the respective light field content on the emissive primitive to achieve higher perceived spatial resolution.

Both projectors and displays have a native resolution of 1920x1080, the pixel spacing is approximately 0.27mm. The parallax barrier and the emissive plane are at a distance of 10mm. The spacing between the parallax barrier slits is between 9 and 12 pixels for one frame, and is adjusted according to the displayed scene. Three consecutive frames are used for temporal multiplexing, resulting in perceived parallax barrier spacing of 3 to 4 pixels. The corresponding 9 to 12 views of each parallax barrier consequently can be used to achieve a field of view of 7° to 9.5°. The virtual distances between the two parallax barrier displays are 100mm and 200mm.

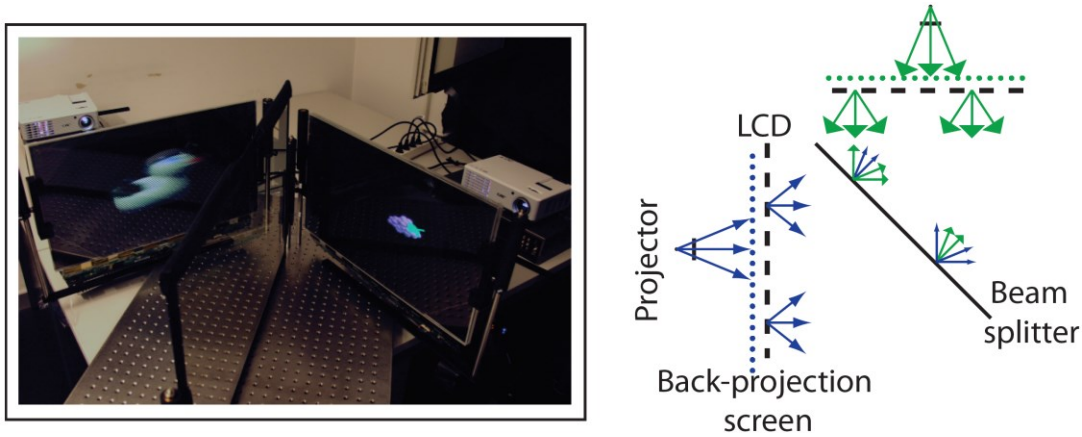

Figure 9: Our spatially multiplexed prototype uses a beamsplitter two overlay two parallax barrier displays.

6. Results

Examples: We demonstrate several examples for both the spatially and temporally multiplexed setups. Figure 1 shows all steps of our algorithm captured on the temporally multiplexed prototype. Figure 5 shows some of the simulation results used for our quantitative analysis. Figure 10 shows real results displayed on the spatially multiplexed prototype with visible parallax between the two views. Our displays are quite unique since an observer is provided with accommodation cues, visible in Figure 11, as well as binocular cues and motion parallax. In addition to this, view-dependent effects can be observed clearly and they add to the depth perception. We believe that the superimposed spatial modulator does not significantly influence the accommodation cues.

Component Limitations: Our beam-splitter setup as well as the time multiplexed setup is limited in terms of possible size and scalability. As shown by [2], the maximum possible number of layers is limited by the finite switching speed of the layers, and the projector refresh rate. In addition, the dynamic range of the display is limited. In order to achieve constant brightness across the displayed light field, the lines in parallax patterns must be brighter than the parts rendered using the emissive layers only. Furthermore, the PDLCD panels are maximally 80% transparent and can only switch at 60Hz. These could be replaced by more-transparent and faster switching panels, as

shown by [13]. In addition, common LCD panels take several milliseconds to switch from white to black, causing shadowing. Finally, transmission of LCD layers is typically less than 10%, which makes the stacking of many LCD layers impractical. Much faster switching panels exist, such as the π-cell, and there is research on large-size, sub-millisecond switching modulators.

Limitations of the Algorithm: Our light field decomposition assumes knowledge of the scene depth, and is so far restricted to synthetic scenes. Our algorithm could work well with pre-recorded light fields, as long as a sufficiently accurate and dense depth map can be computed. Furthermore, we cannot currently handle transparent or semi-transparent scene elements. Finally, the spatially-varying modulators assign fully blocked or transparent states only. Taking advantage of the intermediate states could, in principle, improve the overall bandwidth.

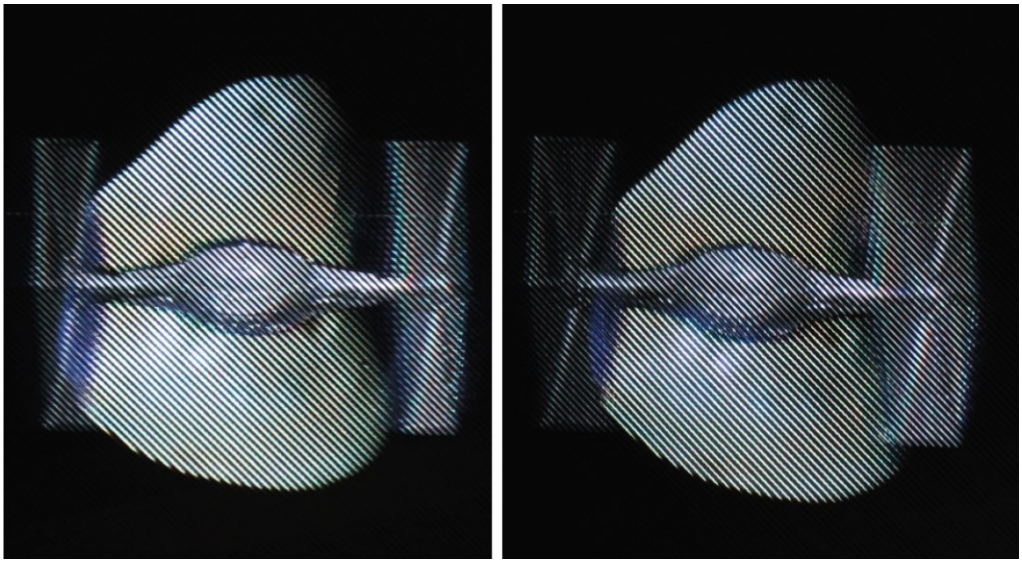

Figure 10: Two views captured on our spatially multiplexed prototype with clearly visible parallax and proper occlusions. The spaceship is rendered on the front layer where to moon is displayed by the layer in the back.

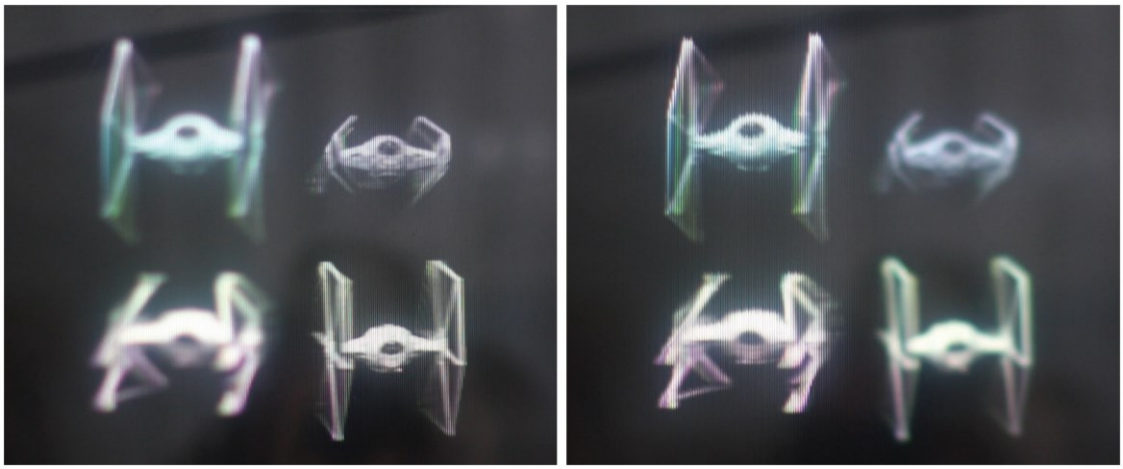

Figure 11: Multi-planar plenoptic displays provide good accommodation cues as visible in these images, captured on our spatially multiplexed prototype with different camera focus.

7. Conclusion

We have introduced a general concept of multi-planar plenoptic displays. These display systems fuse multiple emissive and spatially modulating layers. First, we have presented a mathematical framework to analyze light transport for these displays. Second, we have described a rendering algorithm that takes as input a 3D scene and drives a given multi-planar system. Next, we have conducted an error analysis for multi-planar plenoptic displays. We then discussed practical issues of designing and building different display configurations. We demonstrate examples both in a simulation as well as on our two physical prototypes. Figure 1 shows all steps of our algorithm recorded on our multi-planar plenoptic display, each step decreasing the difference to the input light field. Figure 5 shows some of the simulated results that are used in our quantitative error analysis, supporting our insights about required number of layers. Though limitations imposed by current available hardware we believe our approach to suit a certain range of applications and will get more involved with upcoming technologies.

8. References

[1] Annen, T., Matusik, W., Pfister, H., Seidel, H.-P., and Zwicker, M. "Distributed rendering for multiview parallax displays". In Stereoscopic Displays and Applications, Proceedings of SPIE Vol. 6055 (2006).

[2] Barnum, P.C., Narasimhan, S.g., and Kanade, T. "A multi-layered display with water drops". In SIGGRAPH, (2010).

[3] Bell, G. P., Craig, R., Paxton, R., Wong, G., and Galbraith, D. "Beyond flat panels: Multi-layered displays with real depth". In SID Symposium Digest of Technical Papers, 39, 1, p. 352–355 (2008).

[4] Chai, J.-X., Tong, X., Chan, S.-C., and Shum, H.-Y. "Plenoptic sampling". In Proceedings of SIGGRAPH'00, p. 307–318 (2000).

[5] Coissart, O. S., Napoli, J., Hill, S. L., Dorval, R. K., and Favalora, G. E. "Occlusion-capable multiview volumetric three-dimensional display". Applied Optics 46, p. 1244–1250 (2007).

[6] Durand, F., Holzschuch, N., Soler, C., Chan, E., and Sillion, F. X. "A frequency analysis of light transport". In SIGGRAPH, p. 1115-1126 (2005).

[7] Favalora, G.E. "Volumetric 3D Displays and Application Infrastructure". In Computer, 38, 8, p. 37 – 44, (2005).

[8] Ives, F. "Parallax stereogram and process for making same". US Patent No. 725,567, (1903).

[9] Jones, A., McDowall, I., Yamada, H., Bolas, M., and Debevec, P. "Rendering for an interactive 360 light field display". ACM Transactions on Graphics 26, 3, (2007).

[10] Levin, A., and Durand, F. "Linear view synthesis using a dimensionality gap light field prior". In CVPR, p. 1831–1838 (2010).

[11] Lippmann, G.M. "La photographie integrale". Comptes-Rendus 146, p. 446-451 (1908).

[12] Ranieri, R., Heinzle, S., Smithwick, Q., Reetz, D., Smoot, L.S., Matusik, W., and Gross, M. "Multi-layered automultiscopic displays". Computer Graphics Forum 31, 7, p. 2135–2143 (2012)

[13] Sullivan, A. "DepthCube solid-state 3D volumetric display". In SPIE Stereoscopic Displays and Virtual Reality Systems, vol. 5291, p. 279–284 (2004).

[14] Tamura, S., and Tanaka K. "Multilayer 3-D display by multidirectional beam splitter". Applied Optics 21, p. 3659–3663 (1982).

[15] Wetzstein, G., Lanman, D., Hirsch, M., and Raskar, R. "Tensor Displays: Compressive Light Field Synthesis using Multilayer Displays with Directional Backlighting". ACM Transactions on Graphics 31, 4, (2012).

[16] Zwicker, M., Matusik, W., Durand, F., and Pfister, H. "Antialiasing for automultiscopic 3D displays". In Eurographics Symposium on Rendering (2006).